Supporting Information

Govern et al. 10.1073/pnas.1000966107

SI Materials and Methods

T-Cell Proliferation. T-cell proliferation was assessed by incubating 1×10^5 naive Rag1$^{-/-}$ B3K506 or B3K508 CD4$^+$ T cells for 48 h with 5×10^5 irradiated C57BL/6 spleen cells and titrating amounts of 3K or 3K variant peptides in 200 μL of RPMI, pulsed with 1 microcurie of [^{3}H]thymidine per well for 18 h, harvested, and counted on a Wallac scintillation counter.

TCR Down-Regulation. In total, 1×10^5 B3K506 and B3K508 Rag1$^{-/-}$ CD4$^+$ T cells were incubated with 5×10^4 bone marrow-derived dendritic cells pulsed with titrating amounts of 3K or variant peptides for 16 h in 200 mL of RPMI. Cells were then washed and labeled with anti-TCR-β-FITC (HAM597), anti-CD69-phycoerythrin, anti-CD4-peridinin chlorophyll protein, and anti-Thy1.2-APC. TCR-β expression was assessed by flow cytometry (FACSCalibur; BD Biosciences) on CD4$^+$ Thy1.2$^+$ cells and analyzed using FlowJo version 8.3 (TreeStar).

Intracellular Cytokine Production. In total, 3×10^5 CD4 B3K506 or B3K508 Rag1$^{-/-}$ CD4$^+$ T cells were stimulated with 1×10^5 C57BL/6 bone marrow-derived dendritic cells pulsed with titrating concentrations of 3K or variant peptides in the presence of GolgiPlug (1 μL/mL; BD Biosciences) for 5 h at 37 °C. T cells were then surface-stained with anti-CD4 and anti-CD8, washed, fixed in 4% (vol/vol) formaldehyde (Fischer Scientific), and stained for intracellular TNF-α using a Cytofix/Cytoperm kit (BD Biosciences) in accordance with the manufacturer's protocol. TNF-α expression was assessed by flow cytometry (FACSCalibur) on CD4$^+$ T cells and analyzed using FlowJo version 8.3.

SPR Measurements of TCR-pMHC Kinetics and Affinities. Soluble IA^b/3K and IA^b/3K peptide variants were expressed and produced using the baculovirus expression system, as previously described (1, 2). K_Ds and binding kinetics for TCRs binding to IA^b/3K and APLs were obtained on BIAcore 2000 and 3000 instruments (BIAcore AB). Data points were collected at 0.2-s intervals and analyzed with Bioeval 4.1 software (BIAcore AB). Scatchard analyses of the equilibrium data were used to determine the dissociation constant (K_D). The kinetic data were used to determine the dissociation rate (k_{off}) and the association rate (k_{on}) were calculated from the K_D and k_{off} ($k_{on} = k_{off}/K_D$).

Tests of Different Models of Ligand Potency and Sensitivity to Model Parameters. ***Tests to determine whether T-ligand potency correlates with TCR-pMHC occupancy when TCRs and pMHCs are membrane-bound.*** T-cell ligand potency does not correlate with the measured K_D (Fig. 3*A*). Even though the K_D measurement of soluble proteins does not describe ligand activity, it is possible that changes in receptor occupancy when TCRs and pMHCs are membrane-bound do describe our data. In this section, we provide an alternate argument against receptor-occupancy (K_D)-based theories. In the main text, we concluded that the affect of K_D on receptor occupancy is weak because of saturation effects (Fig. 4). Thus, for a K_D-based model to explain the wide range of activities seen in our dataset, the effect of receptor occupancy on activity would have to be quite strong.

To assess directly whether changes in receptor occupancy can account for ligand potency, we have compared two quantities: (*i*) the dose–response of a T cell to different concentrations of ligand and (*ii*) the response of the T cell, at fixed concentrations of ligand, to ligands with different K_Ds. Because changes in concentration and K_D lead independently to changes in receptor occupancy, the dose–response curves and the mutation studies provide independent measures of the effect of receptor occupancy on activity. By comparing K_D-based changes in receptor occupancy (comparing different ligands) with concentration-based changes (comparing the same ligand at different concentrations), the impact of K_D can be directly assessed. To do so, we posited that changes in peptide concentration lead directly to changes in receptor occupancy, assuming that TCRs are in great excess and that the additional peptide binds MHC. For example, we assume that a 2-fold increase in peptide concentration leads to a 2-fold increase in pMHC-TCR engagement.

Consonant with our arguments against a pure K_D theory in the main text, the data indicate that the effect of receptor occupancy on activity is not strong enough to explain our data. The dose–response curves indicate that large changes in receptor occupancy are required to increase activity, which are far larger than the difference in receptor occupancies between two peptides with different K_Ds. This can particularly be seen by examining the responses of the B3K506 TCR to two different peptides, IA^b/3K and IA^b/P-1A. The IA^b/3K peptide is more stimulatory for the B3K506 TCR than for the IA^b/P-1A peptide at every concentration of peptide. In particular, at a concentration of 0.0001 μM, the 3K peptide induces 14-fold more proliferation than the P-1A peptide. The 3K peptide also has a stronger K_D (7 and 26 μM, respectively), in apparent agreement with a K_D theory. Its 4-fold higher affinity can lead at most, however, to a 4-fold higher receptor occupancy at each concentration of peptide (Eq. **1**). Because of saturation, the actual increase is probably less. In fact, using estimates of relevant parameters, we predicted in the main text that its receptor occupancy is only 12% higher than the receptor occupancy of the P-1A peptide (Fig. 4).

For the K_D model to explain the differential activity of these two peptides, a 4-fold increase in receptor occupancy must be able to generate a 14-fold increase in proliferation. A 4-fold increase in the concentration of P-1A from 0.0001 μM, however, barely increases its proliferation (2-fold). In fact, the concentration of the P-1A ligand must be increased over 50-fold to recapitulate the activity of the 3K peptide at 0.0001 μM. Even if a 50-fold increase in concentration leads to a smaller increase in receptor occupancy, the gap is quite large.

Because the different affinities in our dataset lead to only small differences in receptor occupancy and peptide activity is not very sensitive to receptor occupancy, K_D theories do not explain our data.

Testing the impact of serial triggering. Because neither K_D nor $t_{1/2}$ models, independently or combined, explained the T-cell activation data, we assessed whether serial triggering could influence ligand potency. The serial triggering hypothesis postulates that an individual pMHC can sequentially trigger multiple distinct TCRs (3, 4). Thus, the faster on-rate of IA^b/3K-binding B3K506 TCRs would lead to a greater number of distinct binding events over the course of the T-cell-APC interaction. Serial triggering of many more TCRs by fast kinetic ligands vs. slow kinetic ligands could lead to an increase in the probability of generating uncharacteristically long-lived interactions.

To test whether serial triggering accounts for the ligand potency of IA^b/3K-reactive T cells, we determined how many more binding events would be required for a strong K_D and fast kinetic ligand to bind an equal number of TCRs for at least 2 s as a medium kinetic and medium K_D ligand. We followed the analysis conducted by Coombs et al. (5). In this model, the number of distinct TCRs bound by a pMHC is as follows:

$$N = \frac{\ln(2)}{t_{1/2}}\left(\frac{K_A c_{TCR}}{1 + K_A c_{TCR}}\right)T$$

The parameter T denotes the total time a pMHC is present in the APC-TCR interface. Because the number of distinct TCRs a pMHC binds depends on the affinity and k_{on} in exactly the same way as the receptor occupancy, the conclusion that serial triggering also does not account for our data is not surprising.

As an example, we compared the responses of the fast kinetic B3K506 TCR binding the IA^b/P-1A ligand and the B3K508 TCR binding IA^b/P5R. These two peptides induce similar activity but have different K_D and binding kinetics. If we assume that TCRs binding pMHC have exponentially distributed dwell times, as in the main text, then to have a similar probability of engaging pMHC for 2 s, the B3K506 TCR would have to generate 26-fold more distinct binding events to the IA^b/P-1A ligand than the B3K508 TCR binding IA^b/P5R. However, the 3.6-fold difference in K_D between the two TCR-pMHC pairs leads to only a 6.5-fold difference in the in number of distinct bound TCRs. The impact of serial triggering on equalizing $t_{1/2}$s becomes worse when a higher $t_{1/2}$ threshold is assumed (Fig. S4*C*), further suggesting that serial triggering cannot lead to significant increases in uncharacteristically long-lived TCR-pMHC interactions. Most importantly, both the B3K506 and B3K508 T cells demonstrate enhanced activity to ligands with increasing $t_{1/2}$. These data indicate that for fast kinetic medium and strong K_D ligands, T-cell activation is negatively correlated with increasing numbers of binding events.

Model and parameter sensitivity analysis. A. Model merging receptor occupancy and dwell time. In the main text, we estimated parameters in Eq. **1** to evaluate whether receptor occupancy and dwell time models could jointly explain our data. Recent arguments suggest that the relevant TCR concentration in Eq. **1** is the effective concentration of TCRs in the synapse, averaged over TCR-rich and TCR-sparse regions, assuming that the TCRs can move freely between the two regions (6). Thus, the concentration of TCRs in the interface between the T cell and APC, c^0_{TCR}, was estimated in the main text by dividing the total number of TCRs on a T cell (10,000 TCRs per T cell) by the total surface area of a T cell (500 μm^2), leading to an estimate of 20 TCRs per square micrometer (7). Within TCR-rich regions (e.g., islands), c^0_{TCR} is locally much higher (80–430 TCRs per square micrometer) (8). Although we have used the lower effective concentration of TCRs, higher concentrations would only improve the robustness of our conclusions, as we demonstrate below.

To convert the measured K_A of TCR-pMHC in solution to K_A when the TCR and pMHC are membrane-bound, we have used a confinement length measured for the 2B4 TCR interacting with the MCC88-103 ligand (1.2 nm, corresponding to a conversion factor of 0.262 nm) (7). Although this conversion has precedent, it is uncertain, as recent research reveals (9, 10). The need for more direct measurements of membrane kinetics has long been acknowledged (11). In particular, one recent study of pMHC-TCR kinetics on the membrane has suggested that k_{on} and k_{off} are faster on the membrane than solution-based measurements suggest and that actin-cytoskeleton-driven membrane motion has a role in tearing apart bonds (10). The role of the membrane in breaking apart bonds as short-lived as those in this study is unclear.

Because the parameters involved in our models are uncertain, we checked to determine if our conclusions were robust to parameter variations. First, we checked the validity of our conclusion that the receptor occupancy is saturated. To do so, we varied the K*, modeling uncertainty both in the concentration of TCRs on the T cell and in likely errors in converting SPR-measured affinities to affinities on the membrane (Fig. S6). If the threshold K_D is weaker than our estimate, even weakly binding peptides will almost always be bound and the conclusion is robust. As the threshold K_D becomes much stronger than our estimate, some of the weaker binding peptides in our sample become unsaturated. Even in these cases, however, it is unlikely that changes in the K_D could compensate for changes in the $t_{1/2}$ in a merged receptor occupancy/dwell time model. The dwell time depends strongly (exponentially) on the $t_{1/2}$, whereas the receptor occupancy depends weakly (sublinearly) on the K_D, even if the system is not saturated (see the arguments in the tests of the pure affinity model).

B. Rebinding. B1. Model sensitivity. In the main text, we applied Bell's model (12) to estimate the importance of rebinding on the membrane. Here, we briefly motivate rebinding models to suggest that our qualitative conclusions are robust to the choice of model.

Once a ligand and receptor debind, we assume that there is some probability they will rebind within a given time interval. Suppose we knew this probability (p). The number of rebindings would then be a geometrically distributed random variable with parameter 1−p, assuming that every rebinding is independent, and the expected number of rebindings would be p/(1−p).

What is the probability p? Clearly, it depends on the time interval over which rebindings are counted. In the case of the interaction between TCRs and pMHCs, we are only interested in those rebindings that occur relatively quickly, before the TCR signaling complex disassembles. Because it is unclear how quickly the TCR signaling complex disassembles, however, models must choose a different measure of "quickness." (Analytically, other measures are also more tractable.) One reasonable approach is to count only those rebindings that occur before the pMHC binds to another TCR for the first time.

In a different approach, Bell's model (12) can be interpreted to count only those rebindings that occur almost immediately, before the receptor and ligand are ever separated by more than a molecular distance. To see this, consider the probability that a pMHC binds to a TCR before diffusing away when it is within a molecular distance of the TCR. For simplicity, we can model the reaction and diffusion as competing exponential processes with rates corresponding to their characteristic rates, which scale as k_{on}/L^2 and D/L^2, respectively, where L is the molecular distance. (Note that k_{on} is expressed on a per molecule basis.) Applying this simple analysis to determine the probability p (13), it is possible to obtain Bell's model (12) (Eq. **2**), within a constant factor.

How sensitive are the conclusions to the particular choice of model? Clearly, the choice of which rebindings to count will affect the quantitative results. Allowing more time for the pMHC and TCR pair to rebind, for example, will lead to larger predictions for the t_a. The qualitative prediction of the model, however, is robust. Independent of the choice of model, the t_a will depend on the $t_{1/2}$ and K_D when k_{on} are low or high, respectively, and on a combination of the two when k_{on} are intermediate. The robustness of this conclusion stems from the fact that it can be motivated independently by simple arguments. When k_{on} are slow, rebinding will not occur and the t_a will depend on the single-interaction $t_{1/2}$. Conversely, when k_{on} are fast, a pMHC and a TCR will rebind many times, essentially equilibrating. As a result, the t_a will depend only on the K_D when k_{on} are large.

B2. Parameter estimates and sensitivity. To evaluate whether rebinding could have an impact on the dwell time of B3K506 or B3K508 TCRs engaging IA^b/3K and APL ligands, we estimated the parameters in Eq. **2**. The diffusivity for a TCR and a pMHC was estimated using published experimental measurements. We used 0.04 and 0.02 $\mu m^2/s$ as typical estimates of the diffusivities of a pMHC (14–16) and a TCR, respectively (17–19). The range of reported diffusivities is from 0.01 to 0.1 $\mu m^2/s$ for pMHCs, with measurements concentrated toward the lower end, and from 0.01 to 0.12 $\mu m^2/s$ for TCRs, although the higher estimates may apply to TCRs outside lipid rafts. We converted our SPR measurements

of k_{on} to k_{on} on the membrane by assuming that affinities on the membrane are proportional to SPR-measured affinities, as in our analysis of receptor occupancy, and, further, by assuming that k_{off} on the membrane are identical to those measured by SPR. Because of limited data, it is generally difficult to convert SPR-measured k_{on} to k_{on} on the membrane (11, 20). A recent study of pMHC-TCR kinetics on the membrane has suggested that k_{on} and k_{off} are faster on the membrane than solution-based measurements suggest and that actin-cytoskeleton-driven membrane motion has a role in tearing apart bonds (10). The role of the membrane in breaking apart bonds as short-lived as those in this study is unclear. Additionally, because faster k_{on} promote rebinding but membrane motion driving the pair apart inhibits rebinding, it is too early to understand how our qualitative results would be affected.

Because of the uncertainty in these parameters, we checked the robustness of our conclusion that rebinding explains the potency of the peptides in our dataset. To do so, we varied the threshold for rebinding, k_{on}*, which models uncertainties in the diffusivities of the TCR and the pMHC and errors in converting SPR-measured k_{on} to k_{on} on the membrane. It is also a rough way of accounting for other factors that might increase or decrease the likelihood of rebinding, such as membrane motion, as well as uncertainty in the model itself. Threefold differences in the threshold k_{on} do not qualitatively affect our conclusions (Figs. S5 and S7). As the threshold for rebinding increases, rebindings become less likely for any given pMHC-TCR pair and the effect of rebinding on the t_a weakens. As long as the rebinding threshold falls within or near the range of k_{on} in our data, it will explain at least part of the difference between the B3K506 and B3K508 TCRs, balancing their K_D and $t_{1/2}$.

Independent of the parameter estimates, we also provided best-fit values in the main text, which, being close to our estimates, reinforced our conclusions. We provide another type of best-fit analysis, based on fitting the models to groups of peptides with similar activity, in Fig. S8 to show this conclusion in another way.

1. Huseby ES, et al. (2005) How the T cell repertoire becomes peptide and MHC specific. *Cell* 122:247–260.
2. Huseby ES, Crawford F, White J, Marrack P, Kappler JW (2006) Interface-disrupting amino acids establish specificity between T cell receptors and complexes of major histocompatibility complex and peptide. *Nat Immunol* 7:1191–1199.
3. Valitutti S, Müller S, Cella M, Padovan E, Lanzavecchia A (1995) Serial triggering of many T-cell receptors by a few peptide-MHC complexes. *Nature* 375:148–151.
4. Wofsy C, Coombs D, Goldstein B (2001) Calculations show substantial serial engagement of T cell receptors. *Biophys J* 80:606–612.
5. Coombs D, Kalergis AM, Nathenson SG, Wofsy C, Goldstein B (2002) Activated TCRs remain marked for internalization after dissociation from pMHC. *Nat Immunol* 3:926–931.
6. Zhu DM, Dustin ML, Cairo CW, Golan DE (2007) Analysis of two-dimensional dissociation constant of laterally mobile cell adhesion molecules. *Biophys J* 92:1022–1034.
7. Grakoui A, et al. (1999) The immunological synapse: A molecular machine controlling T cell activation. *Science* 285:221–227.
8. Dushek O, Coombs D (2008) Analysis of serial engagement and peptide-MHC transport in T cell receptor microclusters. *Biophys J* 94:3447–3460.
9. Tolentino TP, et al. (2008) Measuring diffusion and binding kinetics by contact area FRAP. *Biophys J* 95:920–930.
10. Huppa JB, et al. (2010) TCR-peptide-MHC interactions in situ show accelerated kinetics and increased affinity. *Nature* 463:963–967.
11. Dustin ML, Bromley SK, Davis MM, Zhu C (2001) Identification of self through two-dimensional chemistry and synapses. *Annu Rev Cell Dev Biol* 17:133–157.
12. Bell GI (1978) Models for the specific adhesion of cells to cells. *Science* 200:618–627.
13. DeGroot MH (2002) *Probability and Statistics* (Boston Addison-Wesley) 3rd Ed, p 816.
14. Wade WF, Freed JH, Edidin M (1989) Translational diffusion of class II major histocompatibility complex molecules is constrained by their cytoplasmic domains. *J Cell Biol* 109:3325–3331.
15. Edidin M, Kuo SC, Sheetz MP (1991) Lateral movements of membrane glycoproteins restricted by dynamic cytoplasmic barriers. *Science* 254:1379–1382.
16. Pecht I, Gakamsky DM (2005) Spatial coordination of CD8 and TCR molecules controls antigen recognition by CD8+ T-cells. *FEBS Lett* 579:3336–3341.
17. Sloan-Lancaster J, et al. (1998) ZAP-70 association with T cell receptor zeta (TCRzeta): Fluorescence imaging of dynamic changes upon cellular stimulation. *J Cell Biol* 143: 613–624.
18. Favier B, Burroughs NJ, Wedderburn L, Valitutti S (2001) TCR dynamics on the surface of living T cells. *Int Immunol* 13:1525–1532.
19. Gakamsky DM, et al. (2005) CD8 kinetically promotes ligand binding to the T-cell antigen receptor. *Biophys J* 89:2121–2133.
20. Robert P, Benoliel AM, Pierres A, Bongrand P (2007) What is the biological relevance of the specific bond properties revealed by single-molecule studies? *J Mol Recognit* 20:432–447.

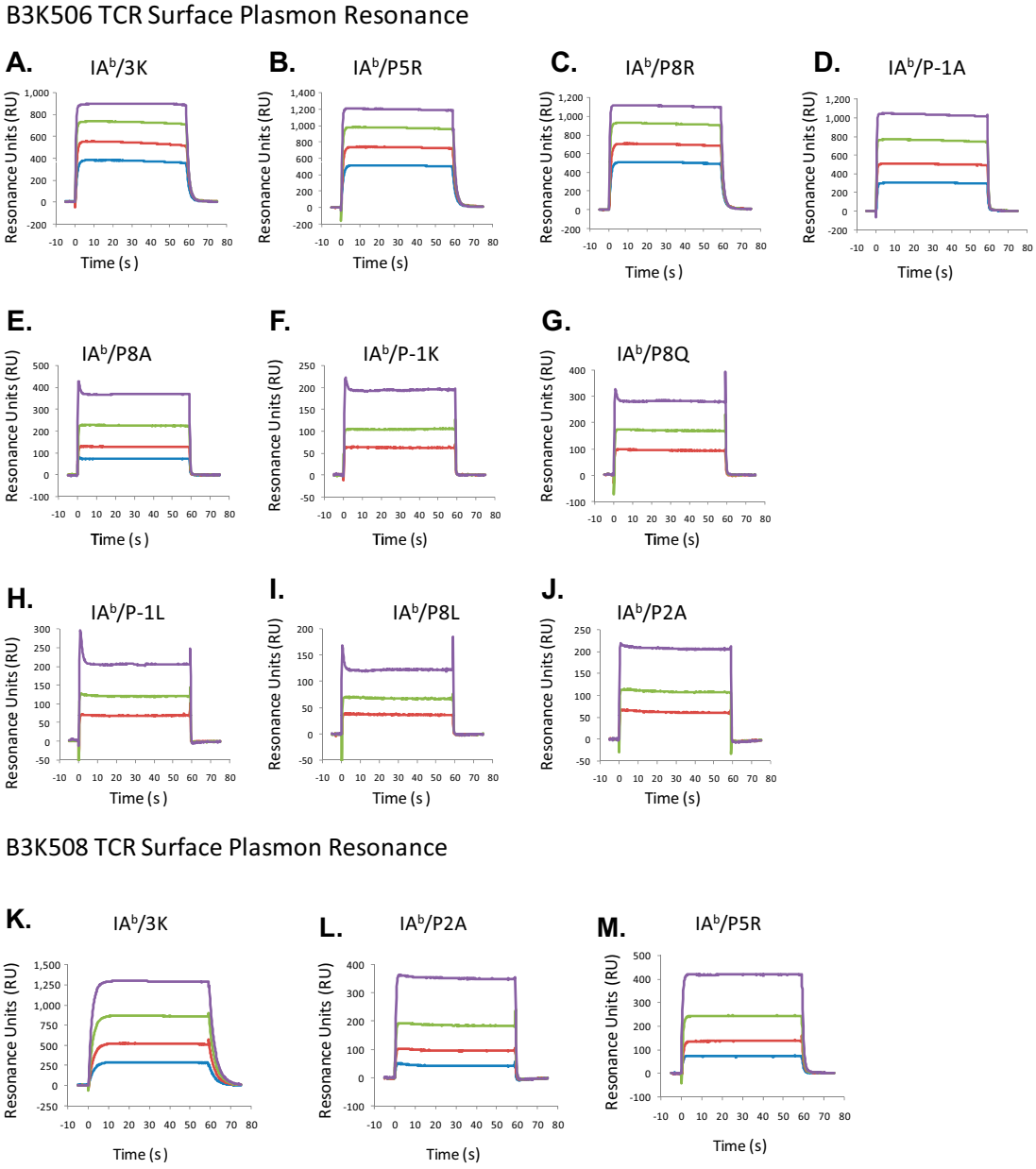

Fig. S1. B3K506 and B3K508 TCRs interact with IA^b/3K and peptide variants with differing rates of association and disassociation. The affinity and kinetics of soluble monomeric IA^b-3K or variant peptide ligands binding to immobilized B3K506 and B3K508 TCRs were analyzed by SPR using BIAcore 2000 and BIAcore 3000 instruments (BIAcore AB). Approximately 2,000 resonance units (RU) of soluble B3K506 TCR was captured on the surface of a CM5 biosensor flow cell by an immobilized anti-Cα mAb, ADO-304. For the B3K506 T cells, soluble IA^b/3K or variant peptides were injected at 20 μL/min for 60 s through a CM5 biosensor flow cell at a concentration of 3K WT (4, 8, 16, and 32 μM) (*A*), P5R (5.6, 11.2, 22.5, and 45 μM) (*B*), P8R (8, 16, 32, and 64 μM) (*C*), P-1A (8, 16, 32, and 64 μM) (*D*), P8A (8, 16, 32, and 64 μM) (*E*), P-1K (12.9, 25.7, and 51.4 μM) (*F*), P8Q (13, 26, and 52 μM) (*G*), P-1L (16, 32, and 64 μM) (*H*), P8L (4, 8, 16, and 32 μM) (*I*), and P2A (4, 8, 16, and 32 μM) (*J*). No specific binding was detected for the P3A, P5A, and P5Q ligands interacting with the B3K506 TCR. For the B3K508 T cells, soluble IA^b/3K or variant peptides were injected at 20 mL/min for 60 s through a CM5 biosensor flow cell at a concentration of 3K WT (4, 8, 16, and 32 μM) (*K*), P5R (5.6, 11.2, 22.5, and 45 μM) (*L*), and P2A (4, 8, 16, and 32 μM) (*M*). Limited binding was detected for the P5A ligand binding the B3K508 TCR at 32 and 64 μM. No specific binding was detected for the P-1A, P8R, P8A, and P3A ligands interacting with the B3K508 TCR. As a control for bulk fluid phase refractive index, the IA^b-3K preparations were also injected through a fourth flow cell with an immobilized irrelevant TCR Ani 2.3 specific for HLA-DR52c. All samples reached equilibrium binding within 10 s. The complex was allowed to dissociate for 60 s between injections. Raw data were corrected for the bulk signal from buffer and IA^b-3K by performing identical injections through a flow cell in which an irrelevant TCR was immobilized. The data were further corrected for the loss of captured TCR during the series of injections based on the observed k_{off} of the TCR from the anti-Cα mAb (~4.5×10^{-4} per second). The data were analyzed with BIAcore Bioeval 4.1 software.

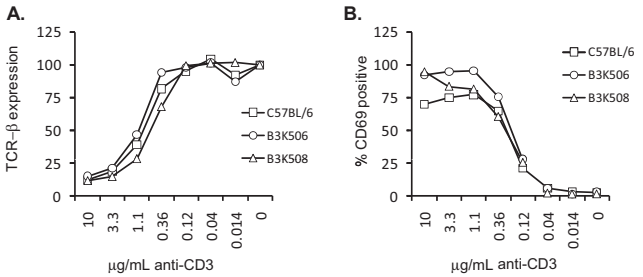

Fig. S2. C57BL/6, B3K506, and B3K508 CD4$^+$ T cells down-regulate TCR expression and up-regulate CD69 expression equivalently in response to titrating amounts of anti-CD3 cross-linking. CD4 T cells were incubated in plates coated with 10 μg/mL anti-CD28, titrating amounts of anti-CD3 for 18 h, and were analyzed by flow cytometry for TCR-β expression (*A*) and CD69 expression (*B*). TCR-β expression is normalized for each T-cell population to the expression at which no activation occurs. Data are the average of three wells per variability and are representative of two independent experiments.

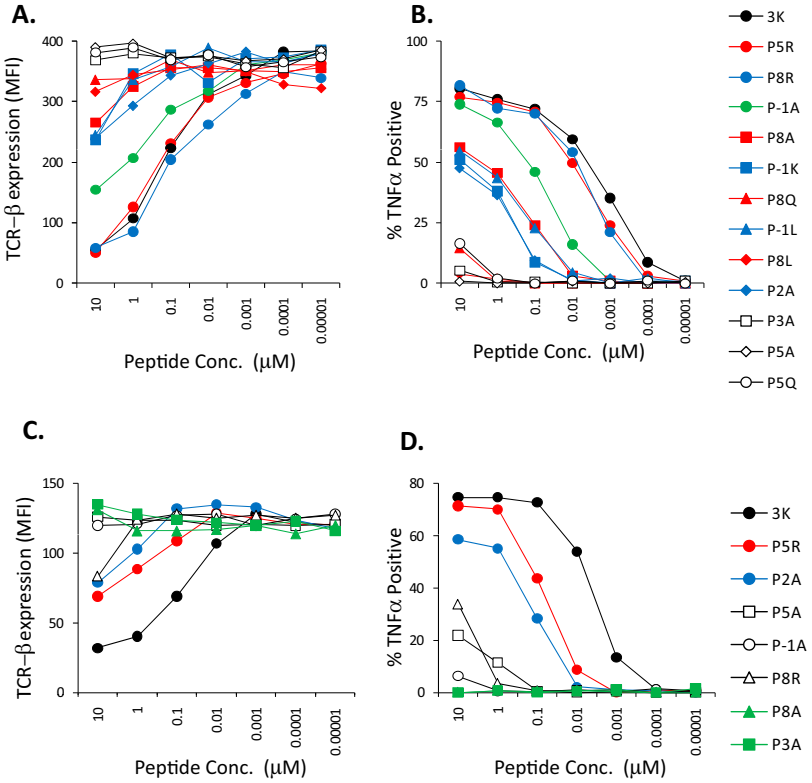

Fig. S3. B3K506 and B3K508 T cells down-regulate TCR expression and produce TNF-α when challenged with high, medium, and low K_D ligands. Naive B3K506 CD4 T cells down-regulate TCR expression (*A*) and produce TNF-α to 3K and APL ligands (*B*). Peptide ligands are listed by decreasing K_D, with the 3K peptide having the strongest K_D and the P5Q peptide having the weakest (undetectable) K_D. Naive B3K508 CD4 T cells down-regulate TCR expression (*C*) and produce TNF-α to 3K and APL ligands (*D*). Peptide ligands are listed by decreasing K_D. Data are representative of at least three independent experiments.

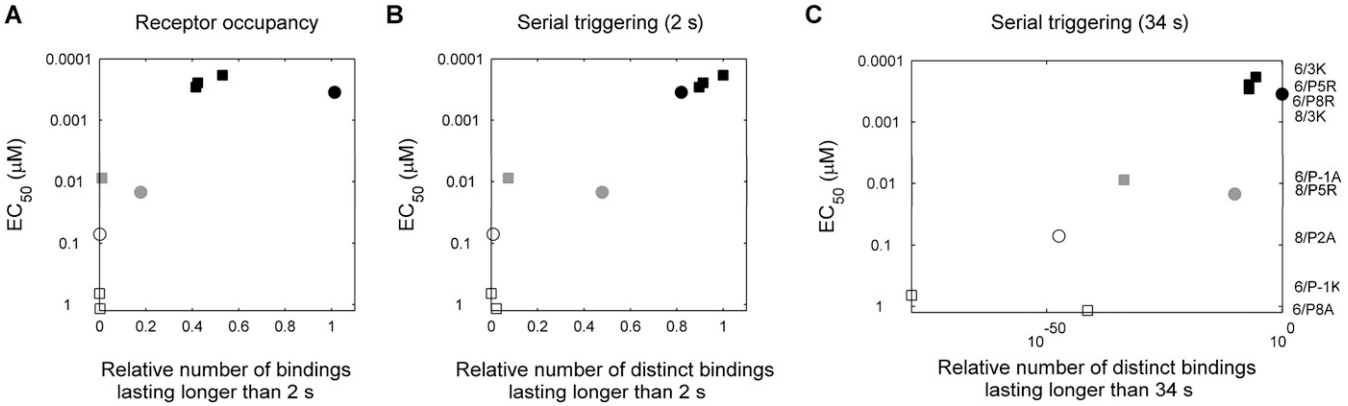

Fig. S4. Evaluating models that correlate ligand potency with the number of long-lived bonds between pMHCs and TCRs. (*A*) Model merging receptor occupancy and dwell time does not explain the activities of the pMHC-TCR pairs. The pMHC-TCR pairs are ranked according to the average number of interactions between them, at any given time, that have lasted longer than 2 s This average number was calculated as the product of two quantities: (*i*) the fraction of peptides bound at any given time, as given in Eq. **1**, and (*ii*) the fraction of such bindings that lasts longer than 2 s, assuming exponentially distributed binding times. The result has been normalized by the B3K508 peptide interacting with the 3K peptide, which is predicted to be the most active. The results are fairly insensitive to the parameter estimates because of the strong (exponential) dependence on the $t_{1/2}$ and the weak (sublinear) dependence on the affinity. (*B* and *C*) Model merging serial triggering and dwell time does not explain the activities of the pMHC-TCR pairs. The pMHC-TCR pairs are ranked according to the number of distinct interactions between them that last longer than a threshold time. The number of interactions is normalized by the number of interactions for the B3K506 TCR interacting with the 3K peptide, which is predicted to be most active. The threshold time required to activate a TCR is assumed to be 2 s (*B*) and 34 s (*C*). (*C*) Note that this panel is on a log scale.

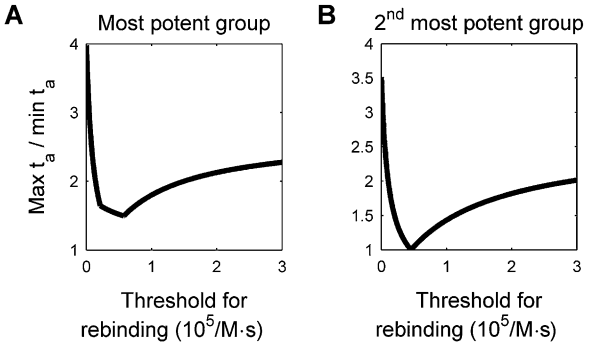

Fig. S5. Determining the optimal rebinding threshold for the data. The variation in t_as within groups of similar activity is plotted against different rebinding thresholds for the most potent group of peptides (*A*) and the second most potent group of peptides (*B*). The optimal thresholds are 60,000/M·s (*A*) and 45,000/M·s (*B*).

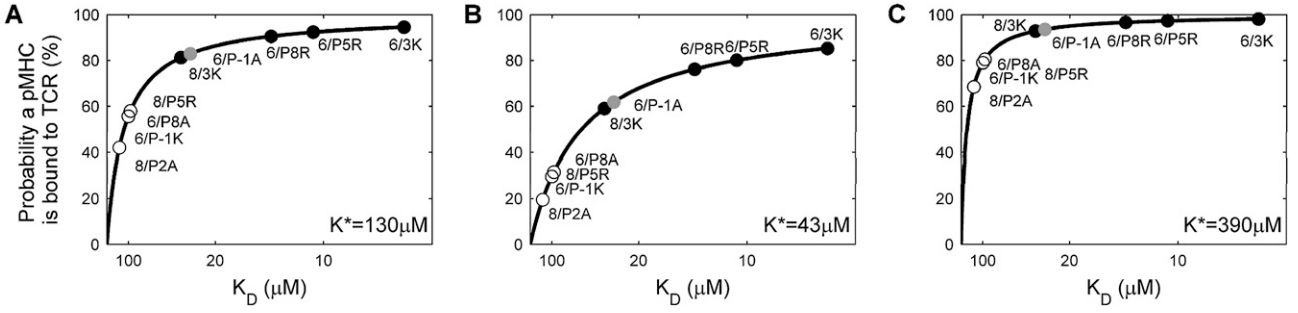

Fig. S6. Sensitivity of receptor occupancy to parameter estimates. The predicted receptor occupancy for each pMHC-TCR pair is plotted, according to Eq. **1**, using a K* of 130 μM as estimated in the main text (*A*) and with a K* three times stronger (43 μM) (*B*) and three times weaker (390 μM) (*C*). The different K*s model uncertainty in the concentration of TCRs on the surface of the cell and the conversion between SPR-measured affinities and affinities on the membrane.

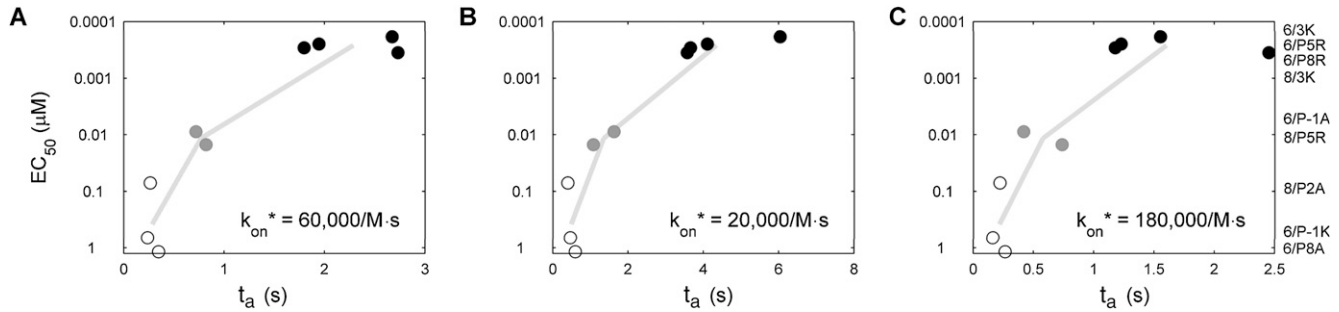

Fig. S7. Sensitivity of rebinding to parameter estimates. Correlations between peptide potency and the t_a are plotted with a rebinding threshold, k_{on}*, of 60,000/M·s (*A*), as estimated in the main text, and with rebinding thresholds three times lower (20,000/M·s) (*B*) and three times higher (180,000/M·s) (*C*). The t_as were determined according to Eq. **2**. The different rebinding thresholds model uncertainty in the diffusivities of the pMHCs and TCRs and the conversion between SPR-measured k_{on} and k_{on} on the membrane.

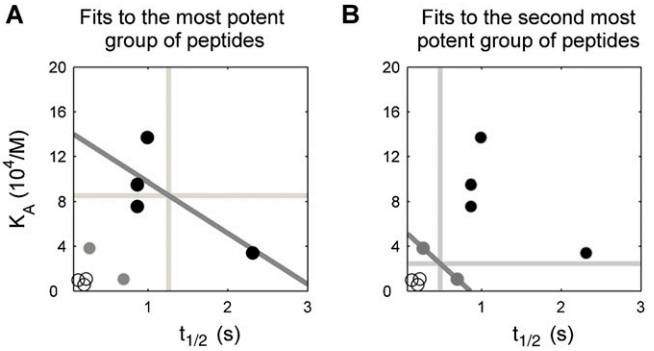

Fig. S8. Models are compared according to their ability to account for peptides with equal activity but different affinities, k_{on}, and $t_{1/2}$s. (*A*) Models are fit to the most potent group of peptides, which all have similar potency. The vertical, horizontal, and diagonal lines correspond to best-fits for the $t_{1/2}$, affinity, and rebinding models, respectively. (*B*) Models are fit to the second most potent group of peptides. The best-fits for the rebinding model correspond to rebinding thresholds, k_{on}^{*}, of 32,000/M·s (*A*) and 45,000/M·s (*B*). These are similar to the best-fits obtained using the techniques in Fig. S5.

Table S1. TCR-ligand K_D, binding kinetics, and T-cell effector functions

TCR	IA^b + 3K mutation	K_D (μM)	k_{on} (1/M·s)	k_{off} (1/s)	$t_{1/2}$ (s)	Proliferation EC_{50} (nM)	TNF-α EC_{50} (nM)
B3K506	WT	7	101,918	0.7	0.9	0.2	3.1
B3K506	P5R	11	74,654	0.8	0.9	0.2	6
B3K506	P8R	13	64,318	0.8	0.8	0.3	7
B3K506	P-1A	26	101,731	2.6	0.3	9	68
B3K506	P8A	92	33,370	3.1	0.2	1,200	2,210
B3K506	P-1K	101	55,149	5.6	0.1	660	5,500
B3K506	P8Q	114	ND	>5	<0.2	9,800	>10,000
B3K506	P-1L	122	ND	>5	<0.2	710	3,600
B3K506	P8L	256	ND	>5	<0.2	>10,000	>10,000
B3K506	P2A	278	ND	>5	<0.2	750	5,500
B3K506	P3A	>550	ND	ND	ND	>10,000	>10,000
B3K506	P5A	>550	ND	ND	ND	>10,000	>10,000
B3K506	P5Q	>550	ND	ND	ND	>10,000	>10,000
B3K508	WT	29	10,887	0.3	2.2	0.4	6
B3K508	P5R	93	11,048	1.0	0.7	15	87
B3K508	P2A	175	19,914	3.5	0.2	71	530
B3K508	P5A	>550	ND	ND	ND	5,700	>10,000
B3K508	P-1A	>550	ND	ND	ND	>10,000	>10,000
B3K508	P8R	>550	ND	ND	ND	980	>10,000
B3K508	P8A	>550	ND	ND	ND	>10,000	>10,000
B3K508	P3A	>550	ND	ND	ND	>10,000	>10,000

Scatchard analysis of binding data data were used to determine the dissociation constant (K_D). The k_{on} was calculated from the K_D and k_{off} ($k_{on} = k_{off}/K_D$). The $t_{1/2}$ values were calculated using first-order reaction kinetics: $t_{1/2} = \ln(2)/k_{off}$. ND, not determined.